Research Square

Preprints are preliminary reports that have not undergone peer review.
They should not be considered conclusive, used to inform clinical practice,
or referenced by the media as validated information.

Repeated Exposure to Ultrafine Carbon Black Particles Induces Pulmonary Mitochondrial Dysfunction and Alterations in Mitochondrial Acetylation

Rahatul Islam
West Virginia University
Jackson E. Stewart
West Virginia University
Atefeh Razazan
West Virginia University
Salik Hussain
West Virginia University
Dharendra Thapa
dharendra.thapa@hsc.wvu.edu

West Virginia University

Article

Keywords: carbon black, particulate matter, mitochondria, metabolism, lysine acetylation, reactive oxygen species

Posted Date: November 19th, 2026

DOI: https://doi.org/10.21203/rs.3.rs-11529087/v1

License: This work is licensed under a Creative Commons Attribution 4.0 International License.
Read Full License

Additional Declarations: No competing interests reported.

Abstract

Ultrafine carbon black (CB) inhalation is associated with pulmonary inflammation and mitochondrial dysfunction, but its effects on several major mitochondrial processes remain incompletely understood. In this study, we investigated whether repeated CB inhalation disrupts pulmonary mitochondrial substrate utilization, bioenergetics and acetylation pattern; one of the major post-translational modifications in mitochondria. Male C57BL/6J mice were exposed to CB aerosols (10 mg/m^3) for 3 hours daily over four consecutive days as a repeated exposure model. Subsequently, whole-lung lysates were analyzed for changes in mitochondrial substrate utilization, electron transport chain (ETC), redox balance, and protein acetylation. Repeated CB exposure significantly reduced the activities of fatty acid oxidation-associated HADHA and pyruvate metabolism-associated PDH enzymes. CB exposure also altered ETC complex assembly and decreased Complex I and IV activities. These changes were accompanied by increased lipid peroxidation and reduced antioxidant enzyme activities, indicating altered pulmonary redox homeostasis. Furthermore, western blot analysis with immunoprecipitation of lung lysates exhibited heterogeneous lysine acetylation across proteins involved in mitochondrial metabolism and antioxidant defense. Collectively, these findings demonstrate that repeated CB inhalation is associated with several pulmonary mitochondrial enzyme dysfunction, redox imbalance, and acetylation remodeling of mitochondrial proteins.

Introduction

Respiratory diseases represent a major global health concern with ambient air pollution as one of the most modifiable risk factors [1]. The World Health Organization (WHO) estimated that ambient air pollution is responsible for approximately 4.2 million annual premature deaths with 68% due to ischemic heart disease and stroke, 14% due to chronic obstructive pulmonary disease (COPD), 14% due to acute lower respiratory infections, and 4% of deaths due to lung cancers [1]. Fine particulate matter ($PM_{2.5}$) and ultrafine particles (UFPs) contribute significantly to these cardiovascular and respiratory diseases burden worldwide [2–4]. Ultrafine and fine PM efficiently deposit in the distal lung and interact with airway and alveolar cells to initiate biological responses associated with oxidative stress and inflammation [5–7]. As a result, long term exposure to PM and UFPs causes increased risk of cardiorespiratory diseases such as COPD, ischemic heart conditions, heart failure, sudden cardiac arrests, irregular heartbeats and atherosclerosis. However, the cellular and molecular mechanisms underlying PM aggravated pathologies are not yet fully understood.

Ultrafine Carbon black (CB) particles are a type of UFP that is extensively used in various industrial applications including pigments, paints, inks/toner and reinforcing agents in polymers [8,9]. Occupational exposure to CB has shown lung and vascular complications and serves as a surrogate model for understanding the toxicological implications of UFP exposure in several studies [10–13]. While these outcomes are well established, the intracellular mechanisms of cardiopulmonary dysfunction by CB exposure are still not fully understood.

Mitochondria are crucial for maintaining cellular homeostasis through their roles in energy production, redox balance, and metabolic regulation [14,15]. In the lung, these functions are essential for sustaining epithelial integrity and supporting immune responses. Although CB-mediated toxicological effects on the lungs are reported in several prior studies, very few of those have extensively focused on CB-induced mitochondrial dysfunction [16–18]. Thus, we have minimal understanding about how CB inhalation influences mitochondrial function in the lung, particularly mitochondrial metabolism or bioenergetic efficiency. In addition, mitochondrial function is influenced by post-translational modifications like lysine acetylation, which can dynamically modulate the activity of enzymes involved in substrate utilization, electron transport, and antioxidant defense [19–22]. This process is mediated by the balance between mitochondrial acetyltransferase GCN5L1 and deacetylases SIRT3 which coordinate metabolic flexibility and stress responses [20,23]. Dysregulation of this acetylation network has been implicated in multiple pathological conditions characterized by oxidative stress and metabolic dysfunction [24–26]. Thus, understanding how mitochondrial lysine acetylation is altered in the lung may provide important insights into the progression of CB-induced injury. Thus, in this study we specifically focused on examining the effects of CB exposure in pulmonary mitochondrial function and mitochondrial acetylation. Overall, the objective of the present study was to investigate how repeated inhalation of ultrafine CB affects pulmonary mitochondrial function. Specifically, we examined changes in mitochondrial substrate utilization, electron transport chain activity (ETC), redox status, and protein acetylation in a controlled murine exposure model.

Results

Aerosol characterization

Detailed physicochemical characterization of the CB aerosol, including particle size distribution, morphology, and mass concentration stability, has been also described extensively in our prior work [12,27]. Briefly, bulk Printex 90® carbon black material was aerosolized to generate a stable ultrafine particulate aerosol. Real-time monitoring confirmed consistent aerosol generation throughout the exposure period in ultrafine size range with a SMPS/APS-based count median diameter of 82.9 nm (2.46). ELPI+ based count median diameter of 64.5 nm (2.12) and Moudi-based mass median diameter of 0.90 µm (2.60). Gravimetric assessments verified that the target exposure concentration was reliably achieved and maintained during all exposure periods (10.33 ± 0.80 mg/m^3).

The physicochemical properties of the CB used in this study including primary particle size, surface area, purity, low endotoxin content, and minimal polycyclic aromatic hydrocarbon contamination have been previously reported [12,27]. Importantly, the same aerosol generation system, exposure conditions, and CB batch were used across studies, ensuring direct comparability between the current study and our previously published work.

Repeated CB exposure disrupted pulmonary mitochondrial substrate utilization

To examine the impact of repeated CB exposure in pulmonary mitochondrial metabolism/substrate utilization, we first measured how fatty acid oxidation (FAO) and glucose oxidation (GO) proteins profile and activity is altered in the lungs. As shown in Fig. 1a **& c**, protein expressions of key FAO protein Hydroxy Acyl CoA dehydrogenase (HADHA), were not altered in CB-exposed lungs compared with air-exposed controls. Despite preserved protein expression, activity analysis revealed a significant reduction in HADHA activity in CB-exposed lungs compared to controls (Fig. 1f). Next, to determine whether repeated CB exposure alters GO pathways in the lung, key regulators of pyruvate metabolism were examined. GO is tightly regulated primarily through the pyruvate dehydrogenase (PDH) complex and its regulatory enzymes. As shown in Fig. 1a **& d**, we report a significant increase in the protein expression of phosphorylated PDH (p-PDH), the inactive form of PDH in our repeated CB exposed lung. In addition, protein levels of pyruvate carboxylase (PC) were also significantly increased following CB exposure (Fig. 1a **& e**). Next, we assessed protein levels of PDK4, a negative regulator of PDH. CB-exposed lungs exhibited a significant increase in PDK4 protein abundance relative to air-exposed controls (Fig. 1b **& h**). These findings suggest decreased utilization of pyruvate in our CB-exposed model. Finally, to determine if these changes translated into functional alterations, PDH enzymatic activity was measured. PDH activity was significantly reduced in CB-exposed lungs compared to controls (Fig. 1g) further corroborating our findings above. In summary, these findings indicate disrupted mitochondrial substrate utilization following repeated CB exposure in the lung.

Repeated CB exposure affected mitochondrial electron transport chain assembly and function

Since FAO and GO feed substrates to the ETC complexes for oxidative phosphorylation, we then examined whether these metabolic disruptions impact ETC complex function through its content assembly or activity. To assess the assembly of mitochondrial respiratory complexes, we first analyzed native ETC complexes using BNPAGE. As shown in Fig. 2, CB exposure altered the composition of multiple ETC complexes content assembly compared with air exposed controls. Densitometric analysis revealed significant changes in the assembly of individual complexes, with increases in Complex I, III, and IV and a reduction in Complex II content assembly in CB-exposed lungs (Fig. 2b-e). In contrast, Complex V showed no significant change in its native complex assembly (Fig. 2f).

We next examined whether these changes were reflected in the enzymatic activity of individual ETC subunits. As shown in Fig. 2g-j, despite no changes in Complex V assembly or protein expression, maximal Complex V activity was significantly increased in CB-exposed lung samples (Fig. 3j). In contrast, maximal activities of Complex I and Complex IV were significantly reduced (Fig. 3g, i), while content assemblies were increased for these two complexes under repeated CB exposure (Fig. 2).

Ultimately this dissociation between complex content assembly and enzymatic function suggests that protein content does not drive their activities.

Repeated CB exposure alters pulmonary redox homeostasis

ETC Complex I and III are the major source of mitochondrial ROS production. We then examined whether repeated CB exposure alters pulmonary redox homeostasis. As shown in Fig. 3a, repeated CB exposure resulted in a significant increase in lipid peroxidation in lung tissue, indicated by elevated malondialdehyde (MDA) levels. This suggests enhanced oxidative damage to membrane lipids following repeated CB exposure.

To assess the antioxidant response, we then examined both the expression and activity of key redox regulating enzymes. Protein levels of mitochondrial SOD2, catalase, PRDX3 and GPX1 showed no significant changes in CB-exposed lungs compared with controls **(**Fig. 3b-h**)**. Despite no changes in protein expression, functional assays revealed a consistent reduction in all antioxidant capacity. SOD activity was significantly reduced in CB-exposed lungs compared to control (Fig. 3i) that indicates impaired detoxification of mitochondrial superoxide. Catalase activity was also significantly decreased (Fig. 3j) suggesting reduced capacity to metabolize hydrogen peroxide. In addition, GPX activity was also significantly reduced in our CB-exposed lungs (Fig. 3k), further supporting a broad impairment in antioxidant defense mechanisms which are not regulated by their protein content.

Repeated CB exposure alters pulmonary mitochondrial protein acetylation

Given the observed impairment of mitochondrial metabolism, ETC complexes, and redox protein activities that were not correlated with their protein content, we next examined if the acetylation pattern of lung mitochondrial proteins are altered following repeated CB exposure.

To assess global changes in protein acetylation, lung lysates were probed with a pan–acetyl-lysine (Ac-K) antibody. As shown in Fig. 4a, CB exposure resulted in a distinct alteration in the pulmonary lysine acetylation pattern compared with air exposed controls. Several proteins exhibited reduced acetylation (asterisks), whereas other proteins displayed increased acetylation (hash marks). This indicates a selective hypo- and hyperacetylation of mitochondrial proteins following repeated CB exposure. These findings suggest that CB exposure induces a broad reprogramming of protein acetylation in the lung. Then, to explore potential regulators underlying these acetylation changes, we examined the protein expression of GCN5L1 and SIRT3. As shown in Fig. 4b-e, we didn’t observe any significant alterations in expression of GCN5L1 or SIRT3 in our CB exposed model.

Repeated CB exposure differentially alters acetylation of mitochondrial substrate utilization and antioxidant

enzymes

Based on the global heterogeneous reprogramming of mitochondrial protein acetylation observed in Fig. 4, we next examined whether key enzymes involved in mitochondrial substrate metabolism exhibit altered acetylation following CB exposure. Immunoprecipitation pull-down with a pan-acetyl lysine antibody was used to measure acetylation levels of FAO and GO enzymes. For FAO, acetylation of HADHA was assessed. As shown in Fig. 5a–b, a significant decrease in HADHA acetylation was observed in CB-exposed mice.

We next examined the acetylation level of key GO-related proteins, including PC, PDH, and PDK4. Acetylation of PC was significantly reduced in CB-exposed lungs compared with air controls (Fig. 5c–d) while PDH acetylation was significantly increased in the CB-exposed group (Fig. 5e–F). However, acetylation of PDK4 showed no changes under repeated CB exposure (Fig. 5g–h).

To determine whether repeated CB exposure alters the acetylation status of mitochondrial antioxidant enzymes, we also examined the acetylation status of key mitochondrial antioxidant enzymes. As shown in Fig. 5i-j, acetylation of mitochondrial SOD2 was significantly reduced in CB-exposed lungs compared with air controls. Site-specific analysis further revealed decreased acetylation at the lysine 122 site of SOD2 **(**Fig. 5m-n**)**. These changes occurred in parallel with a reduction in total SOD activity measured in lung tissue. In contrast, acetylation levels of catalase and GPX1 were not altered between air and CB exposed lungs **(**Fig. 5k-l **& o-p)**. Overall, these findings indicate that repeated CB exposure induces selective, enzyme-specific shifts in lysine acetylation across pulmonary mitochondrial metabolic and antioxidant pathways.

Discussion

In this study, repeated CB inhalation induced coordinated pulmonary mitochondrial dysfunction characterized by impaired substrate utilization, disruption of electron transport chain (ETC) function, increased oxidative stress, and selective alterations in mitochondrial protein acetylation. Unlike acute mitochondrial injury, the pulmonary response to repeated CB exposure involved alterations across multiple interconnected mitochondrial processes including mitochondrial metabolism, respiratory chain function, and antioxidant defense. Together, these findings identify mitochondrial dysfunction as a central mechanism underlying pulmonary toxicity following repeated CB exposure.

In this current study, we found that repeated CB exposure causes pulmonary metabolic reprogramming as shown by impairments in the enzymatic activity of key FAO and GO proteins. Mitochondrial metabolism is essential for maintaining pulmonary epithelial integrity and immune function, as FAO and GO provide ATP required for surfactant production, epithelial repair, and immune surveillance [28–31]. Previous studies have shown that CB exposure induces mitochondrial dysfunction in pulmonary cells; however, whether repeated CB exposure disrupts substrate utilization has remained largely unexplored

[12]. Thus, the observed reduction of both HADHA and PDH activity under repeated CB exposure represents compromised mitochondrial substrate utilization.

In this study, we also found that repeated CB exposure causes significant alterations in mitochondrial ETC organization and function in the lung. In pulmonary epithelial and immune cells, efficient coupling between ETC complex assembly and enzymatic activity is essential to maintain ATP production [32,33]. In this study, BN-PAGE analysis revealed altered assembly patterns of multiple ETC complexes in repeated CB-exposed lungs. We found increased content assembly of selective ETC complexes in our CB exposed mice. However, these changes in complex abundance did not translate uniformly into increased enzymatic function in our study. Rather, we found significantly reduced maximal activities of complexes I and IV. Studies have reported complex I, III, and Complex IV as major sites of mitochondrial ROS production under pathological conditions, particularly when electron flux through the ETC is impaired or uncoupled [15,34,35]. Thus, the observed reduction in maximal activities of these complexes in CB-exposed lungs has significant implications for redox balance. Inefficient electron transfer at Complex I can promote superoxide formation within the mitochondrial matrix, while dysfunction at Complex IV can exacerbate upstream electron leakage and increase the lifetime of partially reduced electron carriers [34,36]. Furthermore, the dissociation between increased ETC content assembly and decreased activity suggests that repeated CB exposure induces functional defects in respiratory chain efficiency rather than a simple loss of mitochondrial mass or protein expression. Similar uncoupling between ETC abundance and function has been reported in several prior studies of particulate matter exposure and is increasingly recognized as a hallmark of mitochondrial stress responses to inhaled nanoparticles [6,37,38].

The functional consequences of ETC dysfunction were further reflected by increased oxidative stress in repeated CB-exposed lungs. We observed increased lipid peroxidation and altered antioxidant enzyme activity in the present study. While overall expression of key mitochondrial antioxidant enzymes was not altered, functional assays revealed a significant reduction in total SOD, Catalase and GPX activity in repeated CB-exposed lungs. This finding underscores the concept that redox dysregulation following nanoparticle exposure is not only mediated by protein abundance but also by functional state and regulatory modification of proteins through post-translational modification [39,40].

Given the central role of lysine acetylation in regulating mitochondrial metabolism and ETC function, we next investigated whether repeated CB exposure altered pulmonary mitochondrial acetylation. Lysine acetylation can modulate the activity of enzymes involved in substrate utilization, electron transport, and antioxidant defense by acting as a crucial on-off switch [19,41,42]. In this study, we found that repeated CB exposure causes both hyper and hypo acetylation pattern of protein expression and such mixed acetylation pattern was consistent in the immunoprecipitation study of several mitochondrial proteins involved in substrate utilization or antioxidant defense. Such heterogeneous acetylation responses are consistent with prior reports demonstrating that mitochondrial stress can produce divergent acetylation outcomes depending on enzyme class, mitochondrial localization, and redox environment [41,43]. Mitochondrial acetylation is tightly regulated by the balance between acetyltransferases GCN5L1 and

deacetylase SIRT3 within the mitochondrial matrix [19,20,44,45]. However, in the present study, we didn't see any changes in the protein expression of GCN5L1 and SIRT3 in lungs under repeated CB exposure.

Despite providing comprehensive evidence that repeated CB inhalation disrupts pulmonary mitochondrial substrate utilization, ETC function and redox homeostasis, several limitations should be acknowledged. First, the present study primarily evaluated mitochondrial function from whole tissue lysates and isolated mitochondrial fractions through molecular assays. While these approaches provide mechanistic insight into ETC efficiency, substrate utilization, and antioxidant capacity, they do not fully capture mitochondrial dynamics in intact versatile pulmonary cell populations. Future studies incorporating high-resolution imaging, mitophagy markers, and cell-type–specific analyses will be essential to determine whether repeated CB exposure induces structural remodeling in parallel with the functional impairments observed here. Secondly, this investigation focused on repeated inhalation exposure in a murine model. While this may be relevant for studying mechanistic toxicity, interspecies differences in airway architecture, immune responses, and metabolic regulation must be considered when extrapolating to human exposure scenarios. Additionally, real-world PM exposure often involves complex mixtures of particles, gases, and co-pollutants for longer periods. Although CB is widely employed to investigate the pulmonary toxicity of combustion-derived nanoparticles, previous studies have demonstrated that different particulate species, including titanium dioxide (TiO_2), diesel exhaust particles (DEP), and silica nanoparticles, can induce pulmonary injury through distinct molecular mechanisms despite producing similar pathological outcomes [6,8,38]. Studies also found that co-exposure paradigms like CB with O_3 can exacerbate mitochondrial dysfunction and oxidative injury beyond single-particle effects [12,27]. Therefore, the mitochondrial dysfunction and acetylation remodeling observed in the present study may not be universally applicable to all particulate matter types. Future investigations comparing multiple environmentally relevant particles and complex pollutant mixtures will be important to determine whether the mitochondrial alterations identified here represent common responses to inhaled particulate matter or are specific to CB exposure.

Materials and methods

Exposure system

CB aerosols were delivered to mice via a whole-body inhalation system designed to generate stable ultrafine-particle atmospheres under controlled conditions. The exposure protocol and system components have been previously described in detail [12,46,47]. In brief, carbon black powder (Printex 90, Evonik, Frankfurt, Germany) was aerosolized using a high-pressure acoustical generator (HPAG; IEStechno, Morgantown, WV, USA) and passed through a deagglomeration stage to produce a respirable ultrafine aerosol. The aerosol stream was introduced into a sealed exposure chamber, allowing uniform distribution of particles throughout the exposure environment.

Animals were exposed to either filtered air (control) or CB aerosol following a repeated exposure protocol e.g., 3 h per day for 4 consecutive days. This exposure setting was selected to model subacute, repeated inhalation of a week-long scenario relevant to occupational and environmental settings. Particle size distribution was periodically assessed to confirm maintenance of an ultrafine aerosol throughout the exposure period as described before [12]. Chamber temperature (20–22 ∘C) and relative humidity (50–70%) were maintained within physiological ranges to minimize environmental stressors.

Animal model

We used young male C57BL/6J mice (8–10 weeks of age) obtained from The Jackson Laboratory (Bar Harbor, ME, USA) for the inhalation exposure. Animals were maintained in an Association for Assessment and Accreditation of Laboratory Animal Care International (AAALAC)-accredited facility under a 12 h light/dark cycle with ad libitum access to food and water. All animal procedures were reviewed and approved by the West Virginia University Institutional Animal Care and Use Committee (IACUC; protocol no: 2107044682_R1.4) and were conducted in accordance with institutional guidelines for the care and use of laboratory animal. After the final exposure, animals were returned to their home cages and monitored for signs of distress or toxicity. No differences in body weight, activity, or general health issues were observed between exposure groups during the study period. After 4 days of repeated CB exposure, animals were anesthetized by inhalation of 4–5% isoflurane (Fluriso™, isoflurane USP; VetOne) and subsequently euthanized by cervical dislocation in accordance with the approved IACUC protocol. Lung tissues were then collected for downstream biochemical and mitochondrial analyses.

Protein isolation

For protein isolation from lung tissue, first we fast froze the samples into liquid nitrogen and then mixed with CHAPS lysis buffer (1% CHAPS, 150 mM NaCl, 25 mM HEPES, 150 mM Nacl, pH 7.4) supplemented with protease and phosphatase inhibitor cocktails. Then lysates were incubated on ice for approximately 2 h to ensure complete solubilization of all proteins. Finally, we spun the lysate in a high-speed centrifuge to separate the insoluble debris from the protein-rich fluid. This produces a clear supernatant that we could use for our downstream experiments e.g., Western blotting, immunoprecipitation, and enzymatic activity assays.

Mitochondrial isolation

We have used differential centrifugation protocol for isolating mitochondria from lung tissue. For this, at first 50 mg of lung tissues were excised and rinsed in ice-cold phosphate-buffered saline to remove blood and weighed. Then we transfer the tissues into a pre-chilled homogenization tubes containing Buffer 1 (100 mM KCl, 50 mM MOPS, 5 mM $MgSO_4$, 1 mM EDTA, pH 7.4), with ATP. Tissue-to-buffer volume was maintained at approximately 1:10 (w/v). Then, we homogenized lung samples through a homogenizer until a uniform suspension was obtained. Then the homogenates were centrifuged at 700 × g for 10 min at 4°C to pellet nuclear debris. After isolating nuclear debris, we transferred the supernatant to a new tube and centrifuged again at 10,000 × g for 10 min at 4°C to isolate the mitochondrial fraction. Finally, this mitochondrial pellet was resuspended in KME buffer (100 mM KCl, 50 mM MOPS, 1 mM

EGTA, pH 7.4) containing protease inhibitor cocktail and washed by an additional centrifugation step at 10,000 × g for 10 min. For experiments that require total mitochondrial protein, the final pellet was resuspended in CHAPS lysis buffer. Protein concentration was also determined using a bradford assay prior to use.

Western blotting

We did western blotting to see the protein expression in lung tissue and isolated mitochondrial fractions. Protein samples were prepared in lithium dodecyl sulfate (LDS) sample buffer with reducing agent and resolved on Bolt Bis–Tris SDS–PAGE gels (4–12% gradient or 12%; Life Technologies, Waltham, MA, USA). After running the protein samples in the SDS–PAGE gels through electrophoresis, we transferred the separated proteins onto nitrocellulose membranes (Life Technologies, Waltham, MA, USA). Then membranes were probed with primary antibodies for proteins involved in mitochondrial fatty acid oxidation, glucose oxidation, electron transport chain complexes, redox milieu, and lysine acetylation. Primary antibodies included rabbit anti-CPT1B (Cat #22170), anti-HADHA (Cat #10758), anti-pyruvate carboxylase (PC; Cat #16588), anti-pyruvate dehydrogenase (PDH; Cat #C54G1), anti-PDK4 (Cat #13776), anti-SOD2 (Cat #66474), anti-K122-SOD2 (Cat #214675), anti-catalase (Cat #D5N75), anti-PRDX3 (Cat #10664), anti-GPX1 (Cat # 29329-1-AP), anti-acetyl-lysine (Cat #9814S), anti-GCN5L1 (Cat # HPA021381), and anti-SIRT3 (Cat #D22A3). Antibodies against mitochondrial electron transport chain complex subunits, including NDUFB8, SDHB, ATP5A, MTCO1, and UQCRC2, were detected using a mouse monoclonal antibody cocktail (Cat #ab110413; Abcam, Waltham, MA, USA). Rabbit anti-glutamate dehydrogenase (GDH; Cat #D9F7P) was used as a mitochondrial loading control. Unless specified, antibodies were obtained from Proteintech (Rosemont, IL, USA) or Cell Signaling Technology (Danvers, MA, USA). Following primary antibody incubation, membranes were washed and incubated with fluorescently labeled secondary antibodies (anti-rabbit or anti-mouse IgG conjugated to infrared dyes at 700 nm or 800 nm; Li-Cor Biosciences, Lincoln, NE, USA). Immunoreactive bands were visualized using a Li-Cor imaging system, and band intensities were quantified by densitometric analysis using ImageJ software (version: 1.54g, NIH, Bethesda, MD, USA).

Immunoprecipitation

We performed immunoprecipitation to assess lysine acetylation of mitochondrial metabolic, electron transport chain, and redox-related proteins in lung tissue. Lung lysates were prepared in CHAPS lysis buffer with deacetylase inhibitors, including trichostatin A (100 μM) and nicotinamide (5 mM) to preserve protein acetylation status during sample processing. Then we measure the protein concentrations and use 500 ug of total protein for each immunoprecipitation reaction.

For acetylation pull-down, lysates were incubated overnight at 4°C with a mouse monoclonal pan-acetyl-lysine antibody (Cell Signaling Technology, Danvers, MA) under gentle rotation. Immune complexes were subsequently captured using Protein A + G agarose beads (Cell Signaling Technology) and washed multiple times with CHAPS buffer to minimize nonspecific binding. Bound proteins were eluted by heating in LDS sample buffer with reducing agent at 95°C. Eluted samples were resolved by SDS–PAGE

on 4–12% Bis-Tris Bolt gels and analyzed by western blotting by using protein-specific primary antibodies. A portion of each lysate (39uL) was retained prior to immunoprecipitation to use as an input control to verify target protein expression. Acetylation levels were quantified by densitometric analysis using ImageJ software (version: 1.54g, NIH, Bethesda, MD, USA) and normalized to corresponding input signals.

Blue native PAGE (BN-PAGE)

Blue native polyacrylamide gel electrophoresis (BN-PAGE) was used to assess the assembly and content of mitochondrial electron transport chain (ETC) complexes I–V in lung tissue. Equal amounts of mitochondrial protein were used for all analyses. Briefly, 20 µg of isolated mitochondrial protein was solubilized in 1% digitonin to preserve native protein interactions. Coomassie Blue G-250 was then added to the samples prior to electrophoresis to facilitate charge shift and native separation. After, samples were loaded onto 4–16% Native PAGE gels, and electrophoresis was performed using a two-step cathode buffer system. Initially, gels were run using dark cathode buffer (prepared from 20× Native PAGE buffer and cathode additive diluted in deionized water) at 110–120 V. After approximately 30 min, the dark cathode buffer was replaced with light cathode buffer containing a reduced concentration of cathode additive. Electrophoresis continued until optimal separation of native complexes was achieved. After electrophoresis, gels were fixed in a solution containing 40% methanol and 10% acetic acid for 15 min. Fixed gels were briefly microwaved at 1100 W for 45 s to enhance protein fixation and subsequently destained in 8% acetic acid for 15 min. Finally, native protein complexes were visualized using a dedicated Native PAGE gel imaging system. Band intensities corresponding to individual ETC complexes were quantified by densitometric analysis using ImageJ software (version: 1.54g, NIH, Bethesda, MD, USA).

Enzymatic activity assays

Fatty Acid and Glucose Oxidation Enzymatic Activity

As a representative of fatty acid oxidation, HADHA activity was measured in lung lysates prepared in 1% CHAPS buffer by monitoring NADH oxidation at 340 nm in a microplate reader following addition of acetoacetyl-CoA. Briefly, 8 µg of protein was added to a reaction mixture containing imidazole buffer (pH 7.4) and NADH. Then the reaction was initiated by the addition of acetoacetyl-CoA. The decrease in absorbance at 340 nm that measures NADH oxidation was recorded over time and activity was calculated using a standard NADH curve. To measure overall glucose oxidation, Pyruvate dehydrogenase (PDH) activity was measured using a commercial colorimetric assay kit (DNPH-100; BioAssay Systems; Hayward, CA, USA),) according to the manufacturer's instructions. All activities were normalized to protein concentration.

ETC Complex Activity Assays

Maximal activities of mitochondrial ETC complexes were measured spectrophotometrically in lung lysates, as described before [10]. Protein concentration was determined by bradford assay prior to

analysis. Briefly, Complex I activity was measured by monitoring NADH oxidation at 340 nm in the presence of decylubiquinone. Complex III and IV activities were assessed by measuring cytochrome c reduction or oxidation at 550 nm by using decylubiquinol or reduced cytochrome c, respectively. Complex V activity was measured via NADH oxidation at 340 nm by using a coupled pyruvate kinase/lactate dehydrogenase system. Specific inhibitors (rotenone, antimycin A, KCN, and oligomycin) were included as negative controls. Activities were calculated using established extinction coefficients and expressed as nmol/min/mg protein.

Antioxidant Enzyme Activity Assays

Total superoxide dismutase (SOD) activity was measured using a commercially available colorimetric assay (ab65354; Abcam, Waltham, MA) based on inhibition of superoxide-mediated tetrazolium salt reduction. Catalase activity was quantified using a formaldehyde-based colorimetric assay (Cat#707002; Cayman Chemical, Ann Arbor, MI) by measuring peroxidatic activity in the presence of hydrogen peroxide. Glutathione peroxidase (GPX) activity was also determined using a commercially available coupled NADPH oxidation assay (Cat#703102; Cayman Chemical, Ann Arbor, MI) as per as the manufacturer’s instructions. An overview of the enzymatic activity assays performed in this study is summarized in Table 1.

Table 1
An overview of the enzymatic activity assays of this study

Assay Category	Enzyme / Complex	Sample Type	Readout (λ)	Substrate	Normalization
ETC Bioenergetics	Complex I	Lung lysate	340 nm	NADH → decylubiquinone	nmol/min/mg
ETC Bioenergetics	Complex III	Lung lysate	550 nm	Decylubiquinol → cytochrome *c*	nmol/min/mg
ETC Bioenergetics	Complex IV	Lung lysate	550 nm	Reduced cytochrome *c*	nmol/min/mg
ETC Bioenergetics	Complex V	Lung lysate	340 nm	PK/LDH-coupled NADH oxidation	nmol/min/mg
FAO	HADHA	Lung lysate	340 nm	Acetoacetyl-CoA / NADH	µmol/min/ug
GO	PDH	Lung lysate	Colorimetric	Pyruvate	U/L
Antioxidant	Total SOD	Lung lysate	Colorimetric	Superoxide	% inhibition/mg
Antioxidant	Catalase	Lung lysate	540 nm	H_2O_2 → formaldehyde	µmol/min/ug
Antioxidant	GPX	Lung lysate	340 nm	H_2O_2	nmol/min/ml

Lipid peroxidation assay

Lipid peroxidation in lung tissue was quantified by measuring malondialdehyde (MDA) levels by using a thiobarbituric acid (TBA) based colorimetric assay (CAT# MAK085, Sigma-Aldrich, Saint Louis, MO). Briefly, lung tissues were homogenized on ice in MDA lysis buffer with butylated hydroxytoluene (BHT) to prevent artificial lipid oxidation during processing. After, homogenates were centrifuged to remove insoluble material, and supernatants were used for analysis. MDA in the samples reacted with TBA under high-temperature acidic conditions to form an MDA-TBA adduct. Reaction mixtures were incubated at 95°C for 60 min, cooled to room temperature, and clarified prior to analysis. Absorbance was measured at 532 nm using a microplate reader. MDA concentrations were calculated from a freshly prepared standard curve and normalized to tissue protein content.

Statistical analysis

All statistical analyses were performed using GraphPad Prism software (version 10). Data are presented as mean ± SEM. Experimental groups consist of 3 to 8 animals, depending on the experiments as indicated in the figure legends. We have selected our mice group sizes based on previous studies which provide the statistical power to detect mitochondrial and metabolic alterations following CB exposure

[10,11]. Comparisons between filtered air and CB exposure groups were conducted using unpaired, two-tailed Student's t tests. Statistical significance was defined as $p < 0.05$.

Statements & declarations

Funding

This work was supported by: NIH/NHLBI K99/R00 (HL 146905) to DT and NIH R01 (ES031253) to SH.

Data Availability

All the relevant data that supports the findings of this study are available within the article (and/or) it's supplementary materials.

Author Contributions

Dharendra Thapa contributed to conceptualization, design, supervision and funding acquisition. Salik Hussain contributed to the resources and supervision. Methodology, data curation and formal analysis were performed by Rahatul Islam. The first draft of the manuscript was written by Rahatul Islam and all authors edited and commented on previous versions of the manuscript. All authors read and approved of the final manuscript.

Competing Interests

The author(s) declare no competing interests.

References

1. WHO. *Ambient (outdoor) air pollution*, <https://www.who.int/news-room/fact-sheets/detail/ambient-(outdoor)-air-quality-and-health> (2024).
2. Lelieveld, J., Evans, J. S., Fnais, M., Giannadaki, D. & Pozzer, A. The contribution of outdoor air pollution sources to premature mortality on a global scale. *Nature* **525**, 367-371 (2015).
3. Rajagopalan, S., Al-Kindi, S. G. & Brook, R. D. Air pollution and cardiovascular disease: JACC state-of-the-art review. *Journal of the American College of Cardiology* **72**, 2054-2070 (2018).
4. Brook, R. D. *et al.* Particulate matter air pollution and cardiovascular disease: an update to the scientific statement from the American Heart Association. *Circulation* **121**, 2331-2378 (2010).
5. Li, N., Xia, T. & Nel, A. E. The role of oxidative stress in ambient particulate matter-induced lung diseases and its implications in the toxicity of engineered nanoparticles. *Free radical biology and medicine* **44**, 1689-1699 (2008).
6. Nel, A., Xia, T., Madler, L. & Li, N. Toxic potential of materials at the nanolevel. *science* **311**, 622-627 (2006).

7. Oberdörster, G., Oberdörster, E. & Oberdörster, J. Nanotoxicology: an emerging discipline evolving from studies of ultrafine particles. *Environmental health perspectives* **113**, 823-839 (2005).
8. Boland, S., Hussain, S. & Baeza-Squiban, A. Carbon black and titanium dioxide nanoparticles induce distinct molecular mechanisms of toxicity. *Wiley interdisciplinary reviews: Nanomedicine and nanobiotechnology* **6**, 641-652 (2014).
9. Niranjan, R. & Thakur, A. K. The toxicological mechanisms of environmental soot (black carbon) and carbon black: focus on oxidative stress and inflammatory pathways. *Frontiers in immunology* **8**, 763 (2017).
10. Islam, R. *et al.* Inhalation of Ultrafine Carbon Black-Induced Mitochondrial Dysfunction in Mouse Heart Through Changes in Acetylation. *Cells* **14**, 1728 (2025).
11. Mullen, W. E., Stewart, J. E., Islam, R., Hussain, S. & Thapa, D. Acute Inhalation Exposure to Ultrafine Carbon Black Alters Mitochondrial Substrate Utilization in the Heart. *Environmental Toxicology* (2025).
12. Hathaway, Q. A. *et al.* Transcriptomics of single dose and repeated carbon black and ozone inhalation co-exposure highlight progressive pulmonary mitochondrial dysfunction. *Particle and Fibre Toxicology* **18**, 44 (2021).
13. Hathaway, Q. A. *et al.* Maternal-engineered nanomaterial exposure disrupts progeny cardiac function and bioenergetics. *American Journal of Physiology-Heart and Circulatory Physiology* **312**, H446-H458 (2017).
14. Murphy, M. P. How mitochondria produce reactive oxygen species. *Biochemical journal* **417**, 1-13 (2009).
15. Balaban, R. S., Nemoto, S. & Finkel, T. Mitochondria, oxidants, and aging. *cell* **120**, 483-495 (2005).
16. Yang, M. *et al.* Ultrafine CB-induced small airway obstruction in CB-exposed workers and mice. *Science of the Total Environment* **671**, 866-873 (2019).
17. Vesterdal, L. K. *et al.* Pulmonary exposure to carbon black nanoparticles and vascular effects. *Particle and fibre toxicology* **7**, 33 (2010).
18. Gilmour, P. S. *et al.* Pulmonary and systemic effects of short-term inhalation exposure to ultrafine carbon black particles. *Toxicology and applied pharmacology* **195**, 35-44 (2004).
19. Hebert, A. S. *et al.* Calorie restriction and SIRT3 trigger global reprogramming of the mitochondrial protein acetylome. *Molecular cell* **49**, 186-199 (2013).
20. Scott, I., Webster, B. R., Li, J. H. & Sack, M. N. Identification of a molecular component of the mitochondrial acetyltransferase programme: a novel role for GCN5L1. *Biochemical Journal* **443**, 655-661 (2012).
21. Anderson, K. A. & Hirschey, M. D. Mitochondrial protein acetylation regulates metabolism. *Essays in biochemistry* **52**, 23-35 (2012).
22. Sack, M. N. & Finkel, T. Mitochondrial metabolism, sirtuins, and aging. *Cold Spring Harbor perspectives in biology* **4**, a013102 (2012).

23. BH, A. A role for the mitochondrial deacetylase Sirt3 in regulating energy homeostasis. *Proc Natl Acad Sci USA* **105**, 14447-14452 (2008).
24. Thapa, D. *et al.* GCN5L1 impairs diastolic function in mice exposed to a high fat diet by restricting cardiac pyruvate oxidation. *Physiological reports* **10**, e15415 (2022).
25. Thapa, D. *et al.* Cardiomyocyte-specific deletion of GCN5L1 in mice restricts mitochondrial protein hyperacetylation in response to a high fat diet. *Scientific Reports* **10**, 10665 (2020).
26. Stewart, J. E. *et al.* Cardiomyocyte-specific deletion of GCN5L1 reduces lysine acetylation and attenuates diastolic dysfunction in aged mice by improving cardiac fatty acid oxidation. *Biochemical Journal* **481**, 423-436 (2024).
27. Majumder, N. *et al.* Aerosol physicochemical determinants of carbon black and ozone inhalation co-exposure induced pulmonary toxicity. *Toxicological Sciences* **191**, 61-78 (2023).
28. Crotta, S. *et al.* Repair of airway epithelia requires metabolic rewiring towards fatty acid oxidation. *Nature Communications* **14**, 721 (2023).
29. Kageyama, T., Ito, T., Tanaka, S. & Nakajima, H. in *Seminars in Immunopathology.* 533-547 (Springer).
30. Lu, X. *et al.* The role of fatty acid metabolism in acute lung injury: a special focus on immunometabolism. *Cellular and Molecular Life Sciences* **81**, 120 (2024).
31. O'Neill, L. A. & Pearce, E. J. Immunometabolism governs dendritic cell and macrophage function. *Journal of Experimental Medicine* **213**, 15-23 (2016).
32. Whitsett, J. A. & Alenghat, T. Respiratory epithelial cells orchestrate pulmonary innate immunity. *Nature immunology* **16**, 27-35 (2015).
33. Basil, M. C. *et al.* The cellular and physiological basis for lung repair and regeneration: past, present, and future. *Cell stem cell* **26**, 482-502 (2020).
34. Brand, M. D. & Nicholls, D. G. Assessing mitochondrial dysfunction in cells. *Biochemical journal* **435**, 297-312 (2011).
35. Scialò, F., Fernández-Ayala, D. J. & Sanz, A. Role of mitochondrial reverse electron transport in ROS signaling: potential roles in health and disease. *Frontiers in physiology* **8**, 428 (2017).
36. Kadenbach, B. Intrinsic and extrinsic uncoupling of oxidative phosphorylation. *Biochimica et Biophysica Acta (BBA)-Bioenergetics* **1604**, 77-94 (2003).
37. Xia, T. *et al.* Comparison of the abilities of ambient and manufactured nanoparticles to induce cellular toxicity according to an oxidative stress paradigm. *Nano letters* **6**, 1794-1807 (2006).
38. Schins, R. P. & Knaapen, A. M. Genotoxicity of poorly soluble particles. *Inhalation toxicology* **19**, 189-198 (2007).
39. Fridovich, I. Superoxide radical and superoxide dismutases. *Oxygen and Living Processes: An Interdisciplinary Approach*, 250-272 (1981).
40. Radi, R. Oxygen radicals, nitric oxide, and peroxynitrite: Redox pathways in molecular medicine. *Proceedings of the National Academy of Sciences* **115**, 5839-5848 (2018).

41. Pougovkina, O. *et al.* Mitochondrial protein acetylation is driven by acetyl-CoA from fatty acid oxidation. *Human molecular genetics* **23**, 3513-3522 (2014).
42. Hirschey, M. D. *et al.* SIRT3 regulates mitochondrial fatty-acid oxidation by reversible enzyme deacetylation. *Nature* **464**, 121-125 (2010).
43. Rardin, M. J. *et al.* Label-free quantitative proteomics of the lysine acetylome in mitochondria identifies substrates of SIRT3 in metabolic pathways. *Proceedings of the National Academy of Sciences* **110**, 6601-6606 (2013).
44. Dittenhafer-Reed, K. E. *et al.* SIRT3 mediates multi-tissue coupling for metabolic fuel switching. *Cell metabolism* **21**, 637-646 (2015).
45. Thapa, D. *et al.* Acetylation of mitochondrial proteins by GCN5L1 promotes enhanced fatty acid oxidation in the heart. *American Journal of Physiology-Heart and Circulatory Physiology* **313**, H265-H274 (2017).
46. Majumder, N. *et al.* Oxidant-induced epithelial alarmin pathway mediates lung inflammation and functional decline following ultrafine carbon and ozone inhalation co-exposure. *Redox Biology* **46**, 102092 (2021).
47. Mazumder, M. H. H. *et al.* Lung-gut axis of microbiome alterations following co-exposure to ultrafine carbon black and ozone. *Particle and Fibre Toxicology* **20**, 15 (2023).

Figures

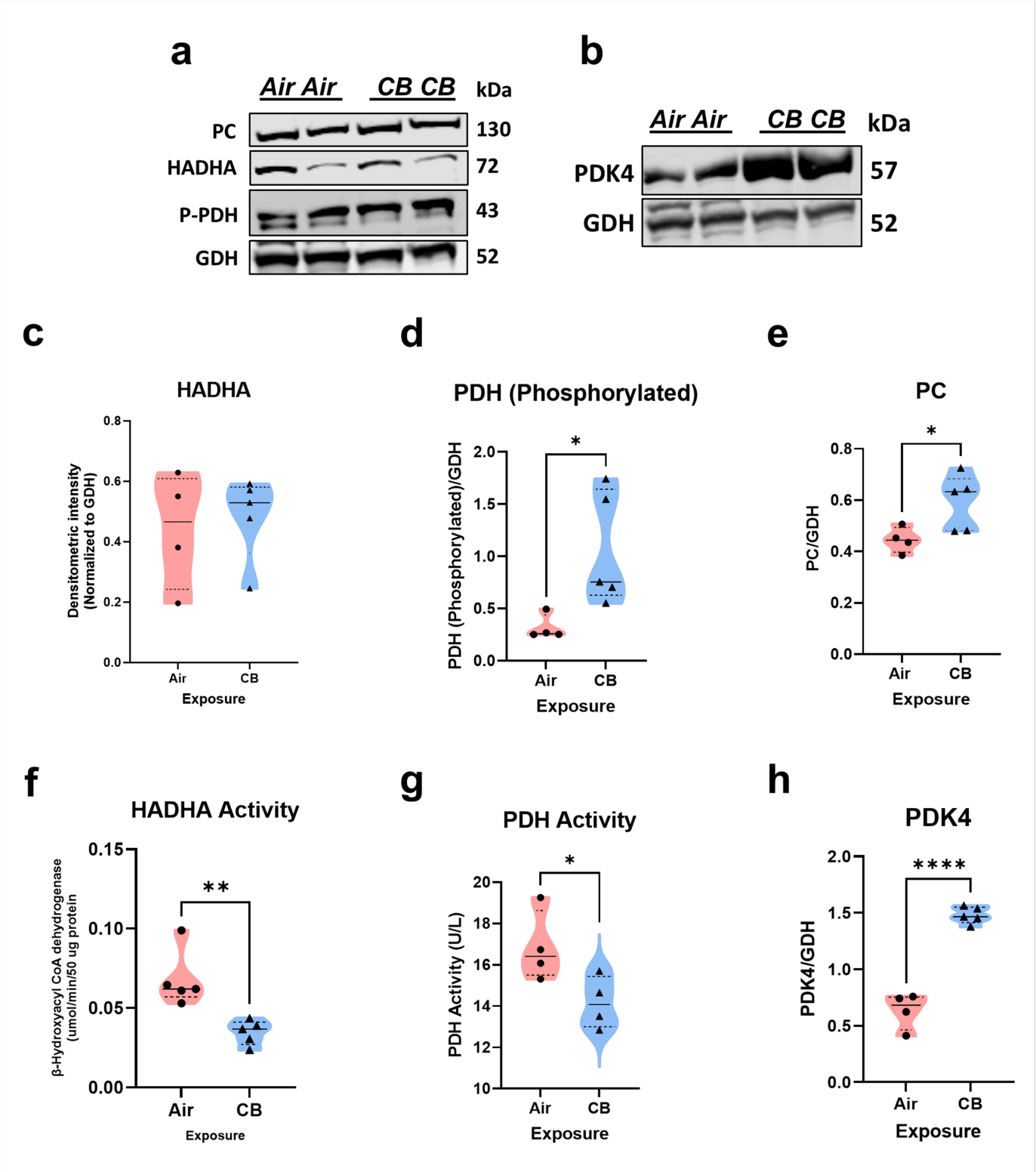


Figure 1

Effects of repeated CB exposure on pulmonary mitochondrial substrate utilization. (a, c) Representative immunoblots with densitometry showing protein expression of key FAO-associated proteins HADHA, with GDH used as a mitochondrial loading control. **(a, d, e)** Representative immunoblots with densitometry showing protein expression of phosphorylated PDH (p-PDH), PC, with GDH as a mitochondrial loading control. **(b, h)** Representative immunoblots with densitometry showing protein

expression of PDK4, with GDH used as a mitochondrial loading control . **(f)** Functional assessment of FAO capacity measured by HADHA enzymatic activity. **(g)** Functional assessment of glucose oxidation capacity measured by PDH activity. Data are presented as mean ± SEM (n = 4–5 per group). Statistical significance was determined using unpaired two-tailed Student's t-test (*p < 0.05, **p < 0.01 **** p < 0.0001 vs. air).

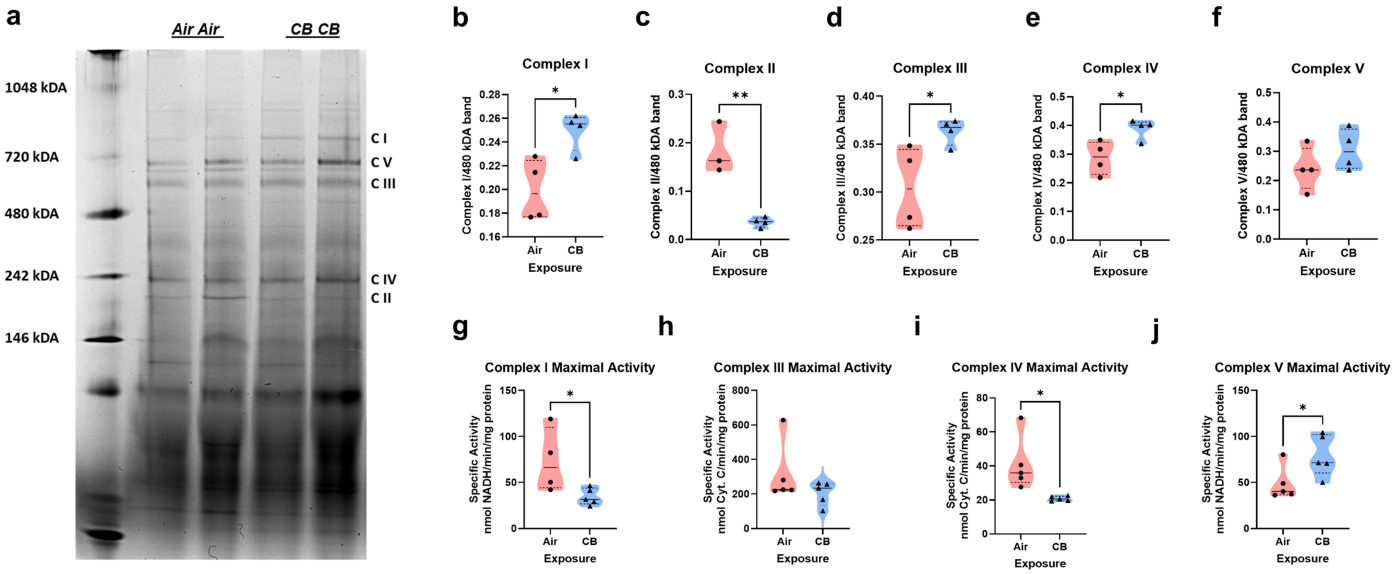


Figure 2 final

Figure 2

Impacts of repeated CB exposure on the assembly and functional activity of mitochondrial ETC complexes in lung tissue. **(a)** Representative BN-PAGE gel showing the distribution and assembly of ETC complexes (Complexes I–V) in lung mitochondrial samples from air and CB exposed mice. **(b–f)** Densitometric quantification of ETC complex assembly normalized to total protein signal, including Complex I, Complex II, Complex IV, Complex III, and Complex V. **(g–j)**Maximal ETC complex activities measured spectrophotometrically. Data are presented as mean ± SEM (n = 4–5 per group). Statistical significance was determined using unpaired two-tailed Student's t-test (*p < 0.05, **p < 0.01 vs. air).

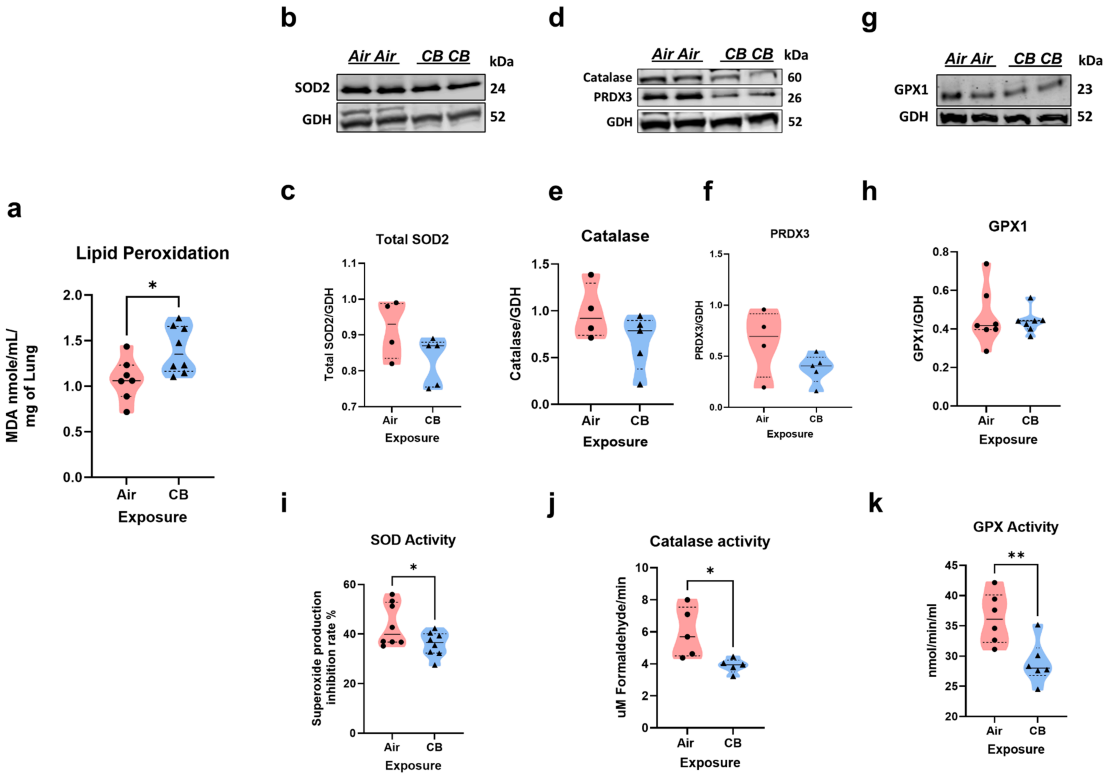


Figure 3 final

Figure 3

Repeated CB exposure's effect on pulmonary oxidative stress and antioxidant enzyme systems. (a) Lipid peroxidation is measured as MDA levels in lung tissue. **(b-h)**Representative immunoblots with densitometry showing protein expression of key antioxidant enzymes, including SOD2, catalase and PRDX3, and GPX1, with GDH as a loading control. **(i–k)** Functional assessment of antioxidant enzyme activities. Data are presented as mean ± SEM (n = 5–8 per group). Statistical significance was determined using unpaired two-tailed Student's t-test (*p < 0.05, **p < 0.01 vs. air).

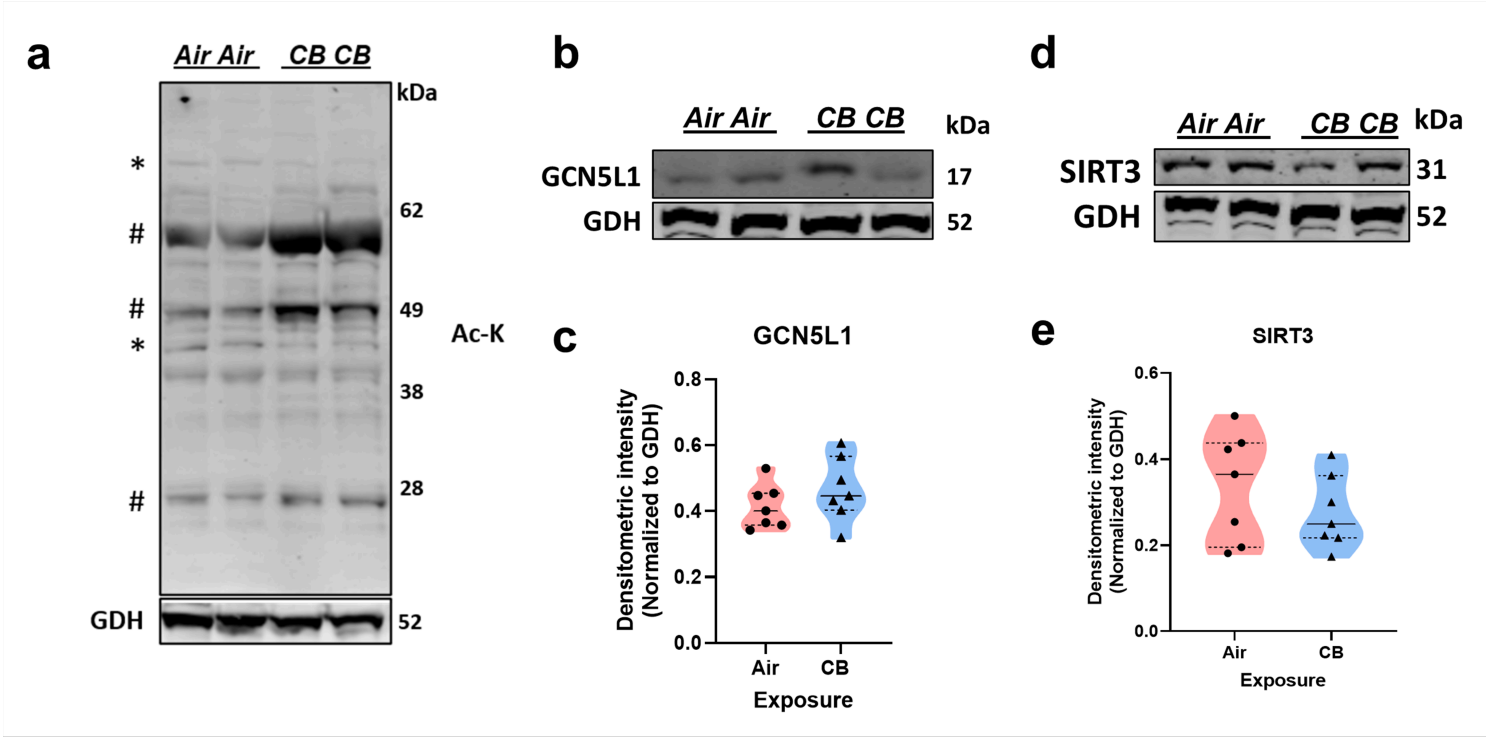


Figure 4

Repeated CB exposure causes heterogenous protein acetylation in lung tissue. (A) Representative immunoblot showing global lysine acetylation (Ac-K) patterns in lung lysates from air and CB exposed mice. ***** Hypoacetylation; # hyperacetylation.

(b, e) Representative immunoblots with densitometry showing protein expression of mitochondrial acetylation regulatory proteins, including GCN5L1 and SIRT3, with GDH as a loading control. Data are presented as mean ± SEM (*n = 7* per group).

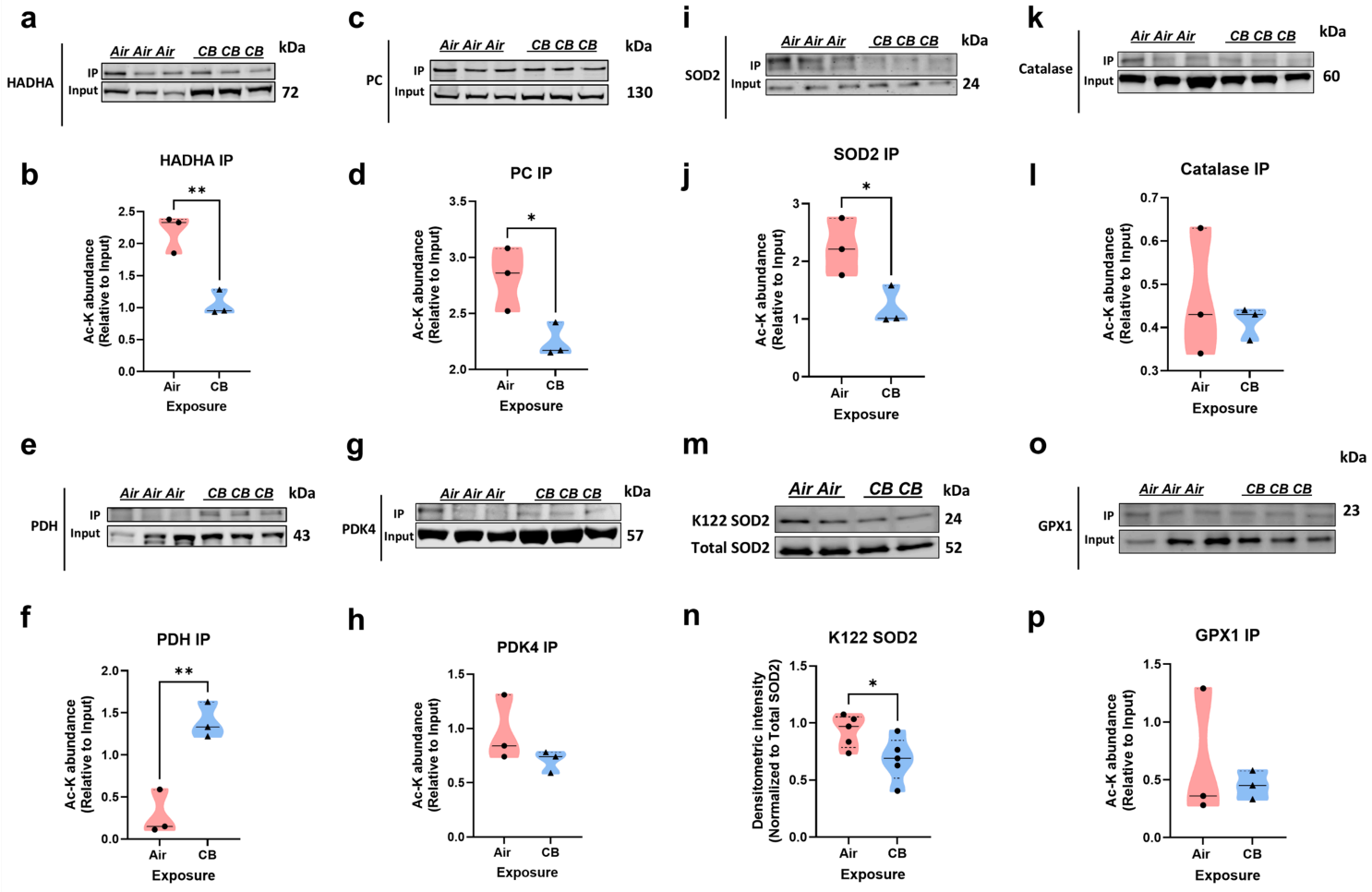


Figure 5

Repeated CB exposure causes heterogenous lysine acetylation of mitochondrial metabolic and antioxidant enzymes assessed by lysine immunoprecipitation. (a-h) Representative immunoblots with densitometry showing acetylation levels of mitochondrial substrate utilization enzymes HADHA, PC, PDH, and PDK4 in air and CB-exposed groups. **(i-p)** Representative immunoblots with densitometry showing acetylation levels of mitochondrial antioxidant enzymes SOD2, Catalase, and GPX in air and CB-exposed groups. Densitometric quantification of acetylated protein abundance (IP) was normalized to input levels. Data are represented as mean ± SEM (*n = 3* per group). Statistical significance was determined using unpaired two-tailed Student's t-test (*p < 0.05, **p < 0.01 vs. air).

Supplementary Files

This is a list of supplementary files associated with this preprint. Click to download.

- SupplementalFullBlotFigures.docx